Results

Single-Cell RNA-Sequencing Reveals Cell Type Heterogeneity and Diet-Induced Alterations in the Intestinal Epithelium

Single-cell RNA-sequencing analysis of small intestinal tissue revealed distinct cell populations and gene expression patters across control diet (CD) and high-fat high-sugat diet (HFHSD) conditions. A total of 27,419 cells passed quality control criteria, with 13,363 cells from CD and 14,056 cells from HFHSD conditions. The average number of genes detected per cell was 3,566 for CD and 3,490 for HFHSD, while the mean UMI count per cell was 18,647 for CD and 20,385 for HFHSD. Unsupervised Leiden clustering and annotation based on known marker genes identified 12 distinct cell clusters (Figure 1a). These clusters represented six main cell types, Intestinal Stem cells (ISC), enterocytes, goblet cells, tuft cells, paneth cells, and enteroendocrine cells. Additionally, progenitor populations were identified for all main cells types excluding ISCs. A cluster of cells that did not express known epithelial cell markers was labelled as ‘Not Annotated’. UMAP visualisation of cells from CD and HFHSD conditions (Figure 1b) showed overall similarity in cluster distribution, indicating sucessful batch correction. However notable differenes were observes in the density of some cell populations, particularly the Paneth cell cluster. Feature pots displaying the average expression of cell type-specific marker genes (Fig 1c) confirmed the identity of annotated clusters. Each cell type exhibited a distinct pattern of marer gene expression, with ISCs sowing high expression of Lgry5, Olfm4, Axin2, Ascl2, Slc12a2, enterocytes displaying expression of Fabp1, Alpi, Apoa1, Apoa4, Lct, Goblet cells displaying expression of Muc2, Tff3, Agr2, Spdef, Klf4, Ccl9, Manf, Paneth cells displaying expression of Lyz1, Mmp7, Defa17, Defa22, and Anf4. Enteroendocrine cells displayed high expression of Neurod1, Neurod2, Insm1, Chga, Chgb, and tuft cells displaying expression of Dclk1, Trpm5, Gfi1b, and Il25. Quantification of cell type proportions between CD and HFHSD conditions (Fig 1d) revealed changes in several cell populations. The ISC population was lower in the HFHSD condition, while enterocyte progenitors showed a higher proportion, suggesting increased cell turnover in the HFHSD condition. Conversely, both tuft progenitors and tuft cells appeared in lower proportions in the HFHSD condition. These trends were consistent with previously published findings using this dataset (cite). Heatmaps of marker gene expression for CD and HFHSD conditions

(Figure 1e) illustrated distinct transcriptional profiles for each of the 12 identified clusters. The heatmaps revealed both shared and diet-specific gene expression patterns across cell types, with certain genes showing differential expression between CD and HFHSD conditions within the same cell type. These data display a comprehensive view of the cellular heterogeneity within the intestinal epithelium as well as some HFHSD induced alterations in cell type proportions and expression profiles. Furthermore, these data display their suitability for further downstream analysis of transcriptional profiling.

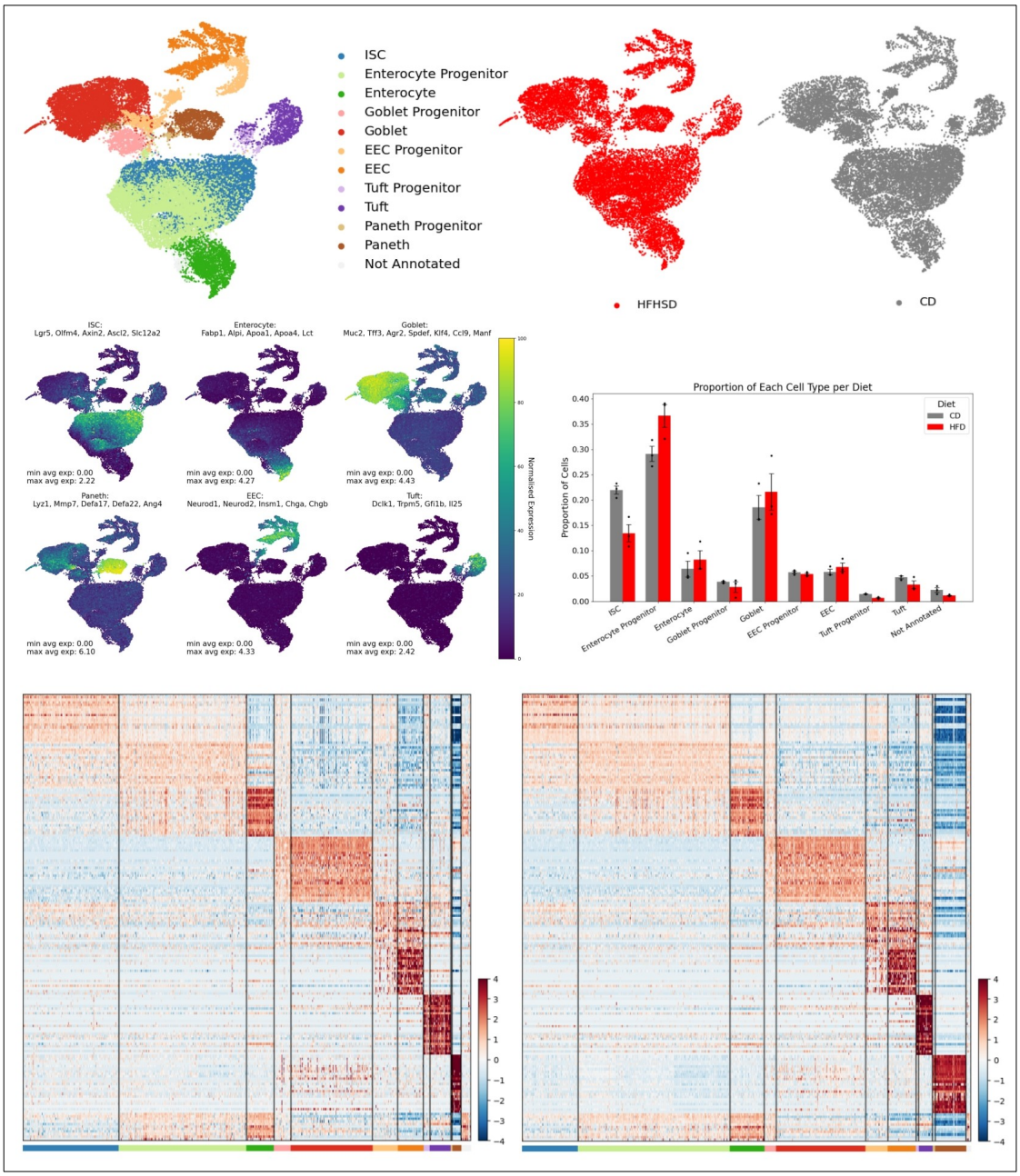

High-Fat High-Sugar Diet Alters ISC Function

Differential gene expression analysis of intestinal stem cells revealed a number of genes with altered expression between the control diet and high-fat high-sugar diet conditions (Figure 2a). Significant changes were observed in genes related to both fat metabolism and cell cycle regulation. Notably, genes involved in fatty acid metabolism and transport showed consistent upregulation. Among these, Fabp1 stood out with one of the highest positive log2 fold changes, while Fabp2, a key intracellular protein involved in the uptake and transport of long-chain fatty acids, also displayed significantly increased expression. Similarly, Hmgcs2, a mitochondrial enzyme essential for the first steps of ketogenesis, exhibited higher expression levels under the high-fat high-sugar diet. Upregulation was also seen in Acot1, an enzyme that facilitates the conversion of acyl-CoAs into fatty acids and CoA, and Scd2, which plays a role in fatty acid biosynthesis. The enzyme Mgll, responsible for breaking down monoacylglycerols into free fatty acids, also showed increased expression.

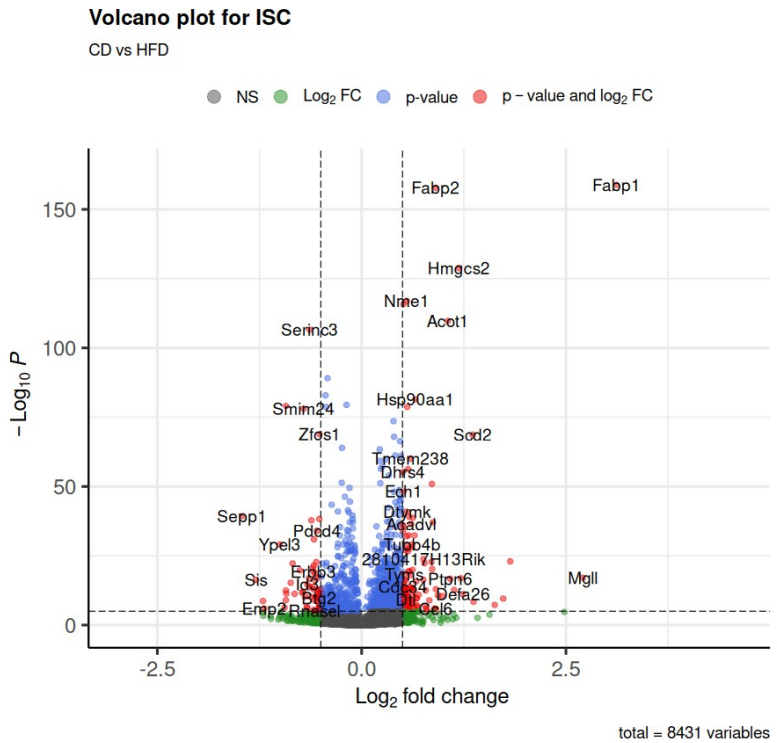

In addition to changes in metabolism-related genes, several genes associated with cell cycle regulation and proliferation were upregulated. Hsp90aa1, a molecular chaperone

known to be involved in cell cycle control, showed a marked increase in expression. Nme1, involved in nucleoside triphosphate synthesis, and Sod2, a mitochondrial protein that protects cells from oxidative stress, also exhibited elevated expression. In contrast, Zfas1, a non-coding RNA linked to cellular differentiation, was downregulated, as was Sepp1, a protein that plays a role in redox balance and epithelial cell proliferation. Additionally, the tumor suppressor Pdcd4 showed significant downregulation, along with Ypel3, a gene associated with the regulation of cellular senescence.

The overall pattern of gene expression changes suggested a predominance of upregulation in response to the high-fat high-sugar diet. This was particularly evident for genes involved in fatty acid metabolism, transport, and cell cycle regulation, as seen in the volcano plot, where a strong trend towards upregulated genes in intestinal stem cells was observed under these dietary conditions.

Gene ontology enrichment analysis

Gene Ontology (GO) enrichment analysis of differentially expressed genes in intestinal stem cells (ISCs) exposed to a high-fat high-sugar diet (HFHSD) revealed significant alterations across Cellular Component (CC), Molecular Function (MF), and Biological Process (BP) categories (Figure X).

The analysis demonstrated a marked upregulation of cell cycle-related processes. Cluster 3 in the BP category showed strong enrichment for terms associated with chromosome separation, mitotic cell cycle, and cell cycle regulation. This pattern was mirrored in the CC section, with enrichment of terms related to chromosomes and mitotic spindles. Complementing these findings, cluster 1 showed enrichment of DNA replication GO terms in the BP category, corresponding to replication fork-related terms in the CC group. The MF category further supported this trend, with upregulation of terms associated with helicase activity, ATP hydrolysis acting on DNA, and single-strand DNA binding.

Mitochondrial function also appeared significantly altered, as evidenced by cluster 6. This cluster showed upregulation of mitochondrial translation and gene expression in the BP category, while the CC section indicated increased expression of mitochondrial ribosome-related terms.

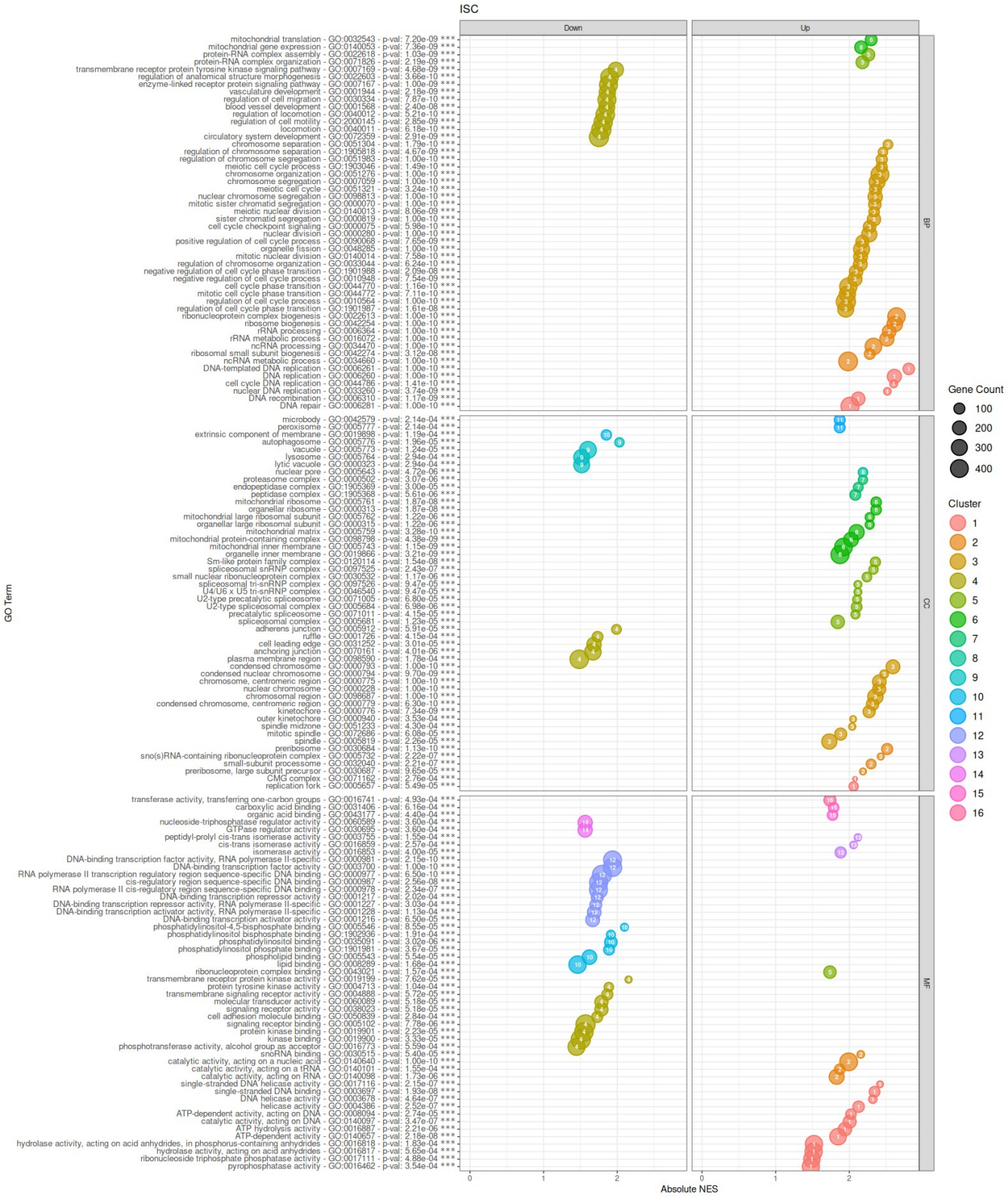

RNA processing mechanisms were notably affected. Cluster 5 revealed upregulation of spliceosome and ribonucleoprotein complex-related terms, particularly in protein-RNA

complex assembly. Similarly, cluster 2 showed increased ribonucleoprotein complex biogenesis, with corresponding upregulation of snoRNA binding in the MF category.

In contrast, the analysis revealed downregulation in specific areas. Cluster 12 showed decreased DNA-binding transcription factor activity specific to RNA polymerase II. Cluster 4 indicated downregulation in genes related to adherens junctions in the CC category, with associated decreases in transmembrane protein kinase activity and cell adhesion molecule binding in the MF category.

In summary, the GO enrichment analysis of ISCs under HFHSD conditions, modeling a prediabetic state, revealed broad upregulation of processes related to cell cycle progression, DNA replication, mitochondrial function, and RNA processing. Conversely, it showed downregulation in specific transcription factor activities and cell adhesion processes. These changes collectively indicate a significant shift in ISC cellular state and function in response to the HFHSD.

The Gene Ontology enrichment network analysis further corroborated and expanded upon the findings observed in the dotplot visualization (Figure X). This network representation integrated Cellular Component, Biological Process, and Molecular Function categories, revealing distinct clusters of functionally related GO terms.

A prominent cluster centered around "regulation of mitotic sister chromatid segregation" emerged, exhibiting positive Normalized Enrichment Scores (NES). This cluster encompassed various cell cycle-related processes, reinforcing the earlier observation of cell cycle upregulation in intestinal stem cells under high-fat high-sugar diet conditions. Similarly, a separate cluster focused on "double-strand break repair via homologous recombination" also displayed positive NES values, further emphasizing the enrichment of DNA replication and repair processes.

Conversely, a cluster associated with "brush border" and "regulation of developmental process" showed negative NES values. This cluster corresponded to the previously noted downregulation of adherens junction-related GO terms, providing additional evidence for altered cell adhesion and developmental processes in the intestinal stem cells.

The enrichment map also highlighted several other functional clusters. Notably, terms related to "mitochondrial translation" and "ribosomal large subunit biogenesis" formed distinct clusters with positive NES values, aligning with the earlier findings of upregulated

mitochondrial and protein synthesis processes. Additionally, clusters associated with "fatty acid binding" and "carboxylic acid metabolic process" were observed, indicating significant alterations in lipid metabolism pathways.

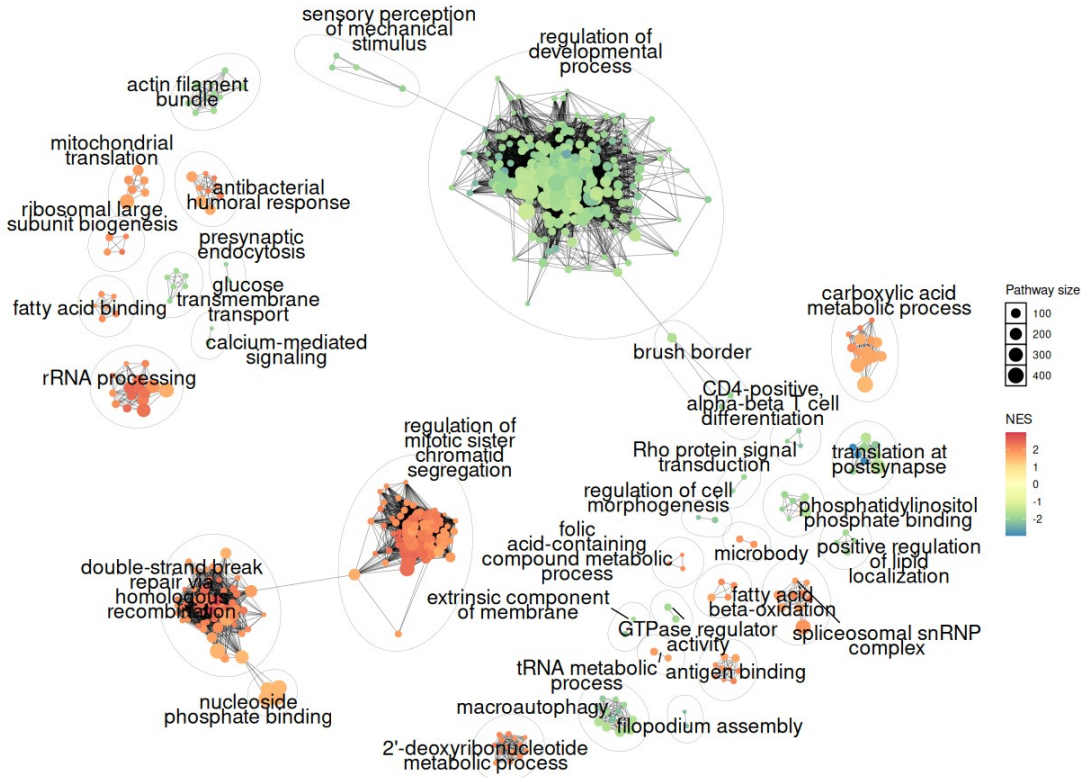

Building upon the GO enrichment analysis, KEGG pathway enrichment analysis of differentially expressed genes in intestinal stem cells (ISCs) exposed to a high-fat high-sugar diet further revealed the functional alterations associated with the prediabetic state (Figure X). The analysis revealed significant enrichment of pathways related to genetic information processing, with DNA replication showing high significance (p = 6.76e-04) and a high gene ratio. This was complemented by enrichment of related pathways including ribosome biogenesis, mismatch repair, and spliceosome. The cell cycle pathway was also significantly enriched (p = 6.33e-03), with most differentially expressed genes upregulated, reinforcing the earlier observations of cell cycle upregulation. Notably, the cell adhesion molecules pathway was enriched (p = 1.29e-02) with a predominance of downregulated genes, demonstrating the impairment of the intestinal barrier in the crypt region. The analysis also highlighted alterations in metabolic processes, with significant enrichment of the PPAR signaling pathway (p = 1.24e-06) and fatty acid metabolism pathways, both

showing a trend towards upregulation. Interestingly, several immune-related pathways showed enrichment, including the Staphylococcus aureus infection pathway and the antigen processing and presentation pathway (p = 8.69e-03), indicating alterations in immune function within the intestinal epithelium under prediabetic conditions. These findings collectively provide a comprehensive view of the molecular and functional changes in ISCs in response to a high-fat high-sugar diet, encompassing alterations in cell cycle regulation, DNA replication, cell adhesion, metabolism, and immune-related processes.

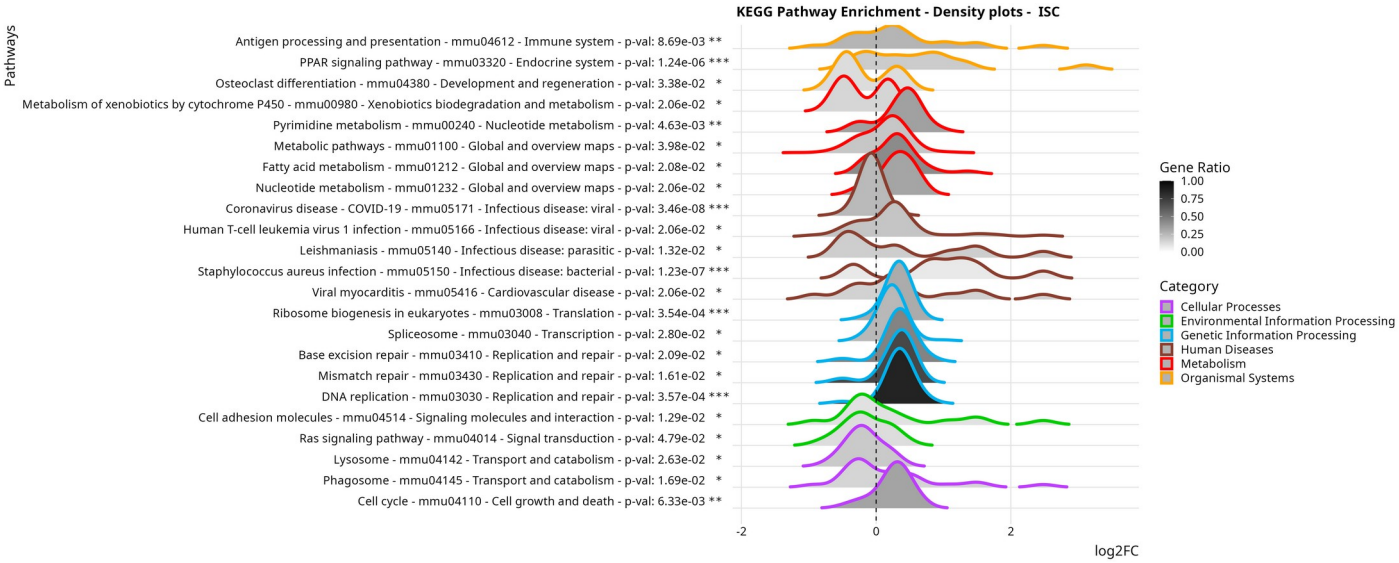

Further examination of the cell cycle pathway through KEGG graphs and heatmaps provided additional insights into the mechanisms of cell cycle alterations in the intestinal epithelium under prediabetic conditions (Figure X). The heatmap analysis revealed that intestinal stem cells (ISCs) and enterocyte progenitors were the most affected cell types within this pathway. ISCs displayed widespread upregulation of cell cycle-related genes, with a slightly attenuated signal observed in enterocyte progenitors. This pattern suggests a rapid proliferation of ISCs followed by differentiation into enterocyte cell types. The KEGG graph visualization of the cell cycle pathway highlighted significant upregulation of key cyclins, including Cyclin D, E, A, and B, as well as Cyclin-dependent kinase 1 (CDK1). The graph also indicated increased expression of CDK4/6, with the regulatory signals predominantly flowing towards DNA replication. These observations at the pathway level corroborate and extend the earlier findings of cell cycle upregulation in ISCs, providing a more detailed view of the specific cell cycle components affected in the prediabetic intestinal epithelium.


Cell cycle
Heatmap of logFC mmu04110 - 76 genes omitted (48.408%)
Sfn
Ppp2ca
Mad2l1
Cdk1
Anapc15
Ccne1
Trip13
Cdkn1c
Aurkb
E2f4
Mcm3
Pkmyt1
Ccnd2
Ccnb2
Ccna2
Cdca5
Trp53
Ccnb1
Mcm5
Bub3
Plk1
Dbf4
Cdc20
Mcm7
Cdc45
Pcna
Fbxo5
Ywhah
Esco2
Mcm2
Anapc11
Mcm6
Mcm4
Ccnd1
Cdt1
Hdac2
Smc3
Cdk4
Hdac1
Orc6
Cdc26
Ppp2r1b
Atm
Ywhaq
Rbx1
Smc1a
Orc4
E2f2
Ywhae
Cdc16
Anapc5
Skp2
Cdc25a
Cdk7
Ptg1
Ppp2r1a
Ywhaz
Bub1b
Ywhab
Ccnh
Anapc7
Cul1
Ywhaq
Anapc16
Crebbp
Fzr1
Tfdp2
Stag1
Anapc13
Cdkn2b
Ep300
Esco1
Wapl
Rb1
Atrx
Pds5a
Gsk3b
Smad3
Cdk6
Stag2
Cdkn1b
1
0.5
0
-0.5
-1
ISC
ENP
ENT
GOB
TUF
EEC

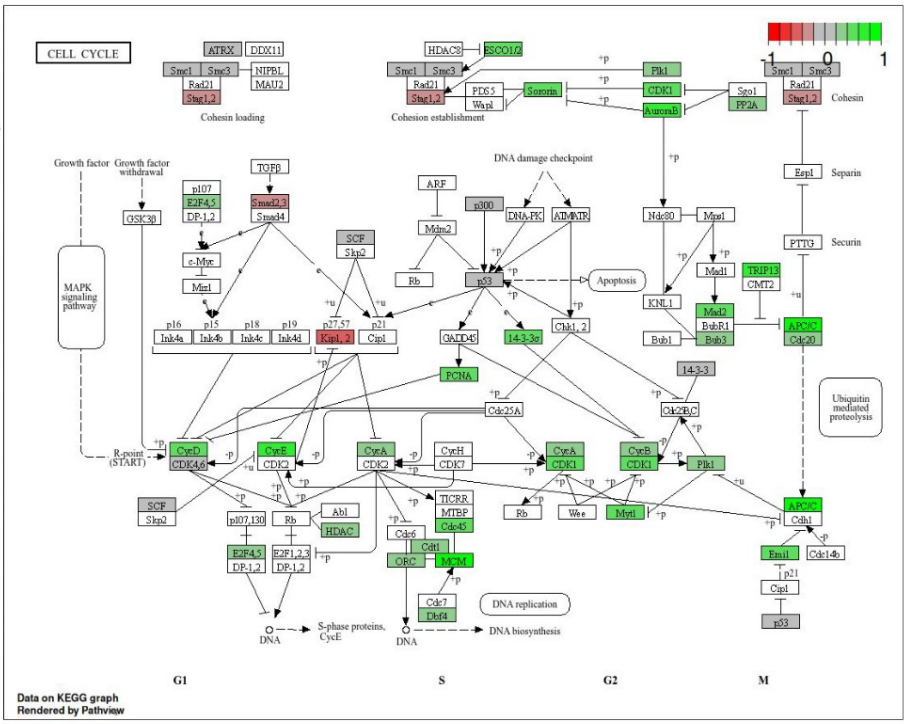
CELL CYCLE
Cohesin loading
Cohesion establishment
Cohesin
Separin
Securin
DNA damage checkpoint
Growth factor
Growth factor withdrawal
MAPK signaling pathway
Apoptosis
R-point (START)
Ubiquitin mediated proteolysis
DNA replication
S-phase proteins, CycE
DNA biosynthesis
G1
S
G2
M
Data on KEGG graph
Rendered by Pathview